Chapter 6: Viscous Flow in Ducts

6.3 Turbulent Flow

Most flows in engineering are turbulent: flows over vehicles (airplane, ship, train, car), internal flows (heating and ventilation, turbo-machinery), and geophysical flows (atmosphere, ocean).

$\underline{V}(\underline{x}, t)$ and $p(\underline{x}, t)$ are random functions of space and time, but statistically stationary flows such as steady and forced or dominant frequency unsteady flows display coherent features and are amendable to statistical analysis, i.e. time and space (conditional) averaging. RMS and other low-order statistical quantities can be modeled and used in conjunction with the averaged equations for solving practical engineering problems.

Turbulent motions range in size from the width in the flow δ to much smaller scales, which become progressively smaller as the $Re = U\delta/\upsilon$ increases.

Fig. 1.1. A photograph of the turbulent plume from the ground test of a Titan IV rocket motor. The nozzle's exit diameter is 3 m, the estimated plume height is 1,500 m, and the estimated Reynolds number is 200×10^6. For more details see Mungal and Hollingsworth (1989). With permission of San Jose Mercury & News.

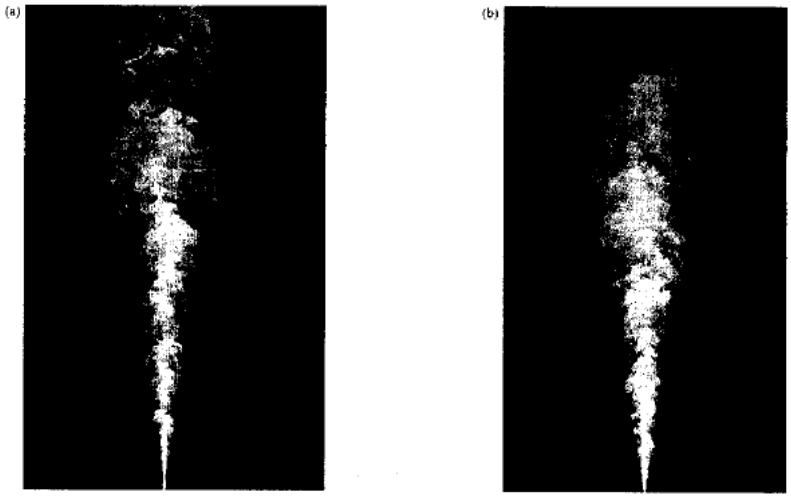

Fig. 1.2. Planar images of concentration in a turbulent jet: (a) Re = 5,000 and (b) Re = 20,000. From Dahm and Dimotakis (1990) .

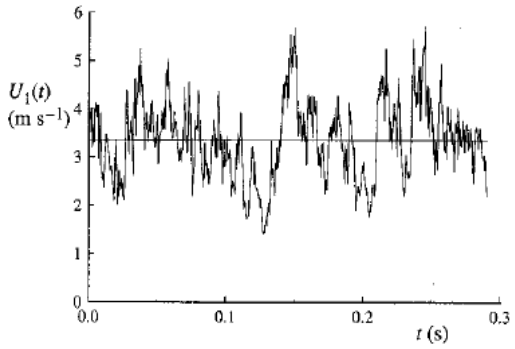

Fig. 1.3. The time history of the axial component of velocity $U_1(t)$ on the centerline of a turbulent jet. From the experiment of Tong and Warhaft (1995).

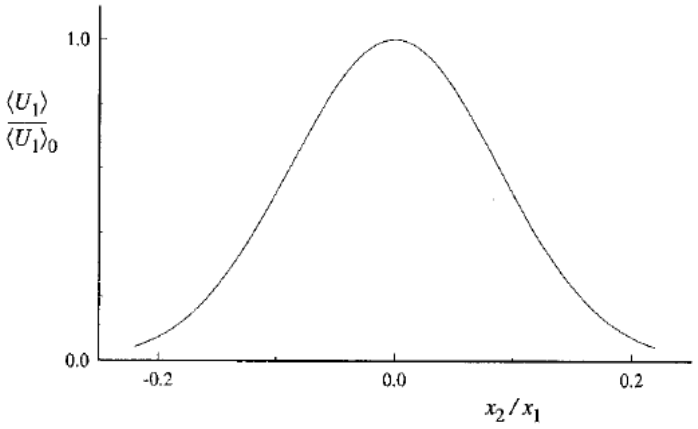

Fig. 1.4. The mean axial velocity profile in a turbulent jet. The mean velocity $\langle U_1 \rangle$ is normalized by its value on the centerline, $\langle U_1 \rangle_0$; and the cross-stream (radial) coordinate x_2 is normalized by the distance from the nozzle x_1. The Reynolds number is 95,500. Adapted from Hussein, Capp, and George (1994).

Physical description:

(1) Randomness and fluctuations:

Turbulence is irregular, chaotic, and unpredictable. However, for statistically stationary flows, such as steady flows, can be analyzed using Reynolds decomposition.

$$u = \bar{u} + u' \qquad \bar{u} = \frac{1}{T}\int_{t_0}^{t_0+T} u\,dT \qquad \bar{u}' = 0 \qquad \overline{u'^2} = \frac{1}{T}\int_{t_0}^{t_0+T} u'^2\,dT \qquad \text{etc.}$$

$\bar{u}$ = mean motion
u' = superimposed random fluctuation
$\overline{u'^2}$ = Reynolds stresses; RMS = $\sqrt{\overline{u'^2}}$

Triple decomposition is used for forced or dominant frequency flows

$$u = \bar{u} + u'' + u'$$

Where u'' = organized oscillation

(2) Nonlinearity

Reynolds stresses and 3D vortex stretching are direct result of nonlinear nature of turbulence. In fact, Reynolds stresses arise from nonlinear convection term after substitution of Reynolds decomposition into NS equations and time averaging.

(3) Diffusion

Large scale mixing of fluid particles greatly enhances diffusion of momentum (and heat), i.e.,

Reynolds Stresses: $-\rho\overline{u'_i u'_j} >> \overbrace{\tau_{ij} = \mu\varepsilon_{ij}}^{viscous\ stress}$

Isotropic eddy viscosity: $-\overline{u'_i u'_j} = \nu_t \varepsilon_{ij} - \frac{2}{3}\delta_{ij}k$

(4) Vorticity/eddies/energy cascade

Turbulence is characterized by flow visualization as eddies, which varies in size from the largest L_δ (width of flow) to the smallest. The largest eddies have velocity scale U and time scale L_δ/U. The orders of magnitude of the smallest eddies (Kolmogorov scale or inner scale) are:

L_K = Kolmogorov micro-scale = $\left[\frac{\upsilon^3\delta}{U^3}\right]^{\frac{1}{4}}$

L_K = O(mm) >> $L_{\text{mean free path}} = 6 \times 10^{-8}$ m
Velocity scale = $(\nu\varepsilon)^{1/4}$ = O(10^{-2}m/s)
Time scale = $(\nu/\varepsilon)^{1/2}$ = O(10^{-2}s)

Largest eddies contain most of energy, which break up into successively smaller eddies with energy transfer to yet smaller eddies until L_K is reached and energy is dissipated by molecular viscosity.

Richardson (1922):

L_δ Big whorls have little whorls
Which feed on their velocity;
And little whorls have lesser whorls,

L_K And so on to viscosity (in the molecular sense).

(5) Dissipation

$\ell_0 = L_\delta$

$u_0 = \sqrt{k}$ $\quad k = \overline{u'^2} + \overline{v'^2} + \overline{w'^2}$

$= 0\,(U)$

$\mathrm{Re}_\delta = u_0 \ell_0 / \upsilon = big$

→ Energy comes from largest scales and fed by mean motion

ε = rate of dissipation = energy/time

$= u_0^2 / \tau_o$ $\quad \tau_o = \ell_0 / u_0$

$= u_0^3 / l_0$ independent υ $\quad L_K = \left[\frac{\upsilon^3}{\varepsilon}\right]^{\frac{1}{4}}$

→ Dissipation occurs at smallest scales

Dissipation rate is determined by the inviscid large scale dynamics.

Decrease in ν decreases scale of dissipation L_K not rate of dissipation ε.

Fig. below shows measurements of turbulence for $Re_x=10^7$.

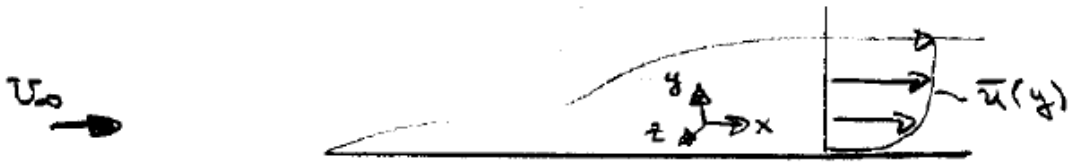

Note the following mean-flow features:

(1) Fluctuations are large ~ 11% U_∞

(2) Presence of wall causes anisotropy, i.e., the fluctuations differ in magnitude due to geometric and physical reasons. $\overline{u'^2}$ is largest, $\overline{v'^2}$ is smallest and reaches its maximum much further out than $\overline{u'^2}$ or $\overline{w'^2}$. $\overline{w'^2}$ is intermediate in value.

(3) $\overline{u'v'} \neq 0$ and, as will be discussed, plays a very important role in the analysis of turbulent shear flows.

(4) Although $\overline{u_i u_j} = 0$ at the wall, it maintains large values right up to the wall

(5) Turbulence extends to y > δ due to intermittency. The interface at the edge of the boundary layer is called the superlayer. This interface undulates randomly between fully turbulent and non-turbulent flow regions. The mean position is at y ~ 0.78 δ.

(6) Near wall turbulent wave number spectra have more energy, i.e. small λ, whereas near δ large eddies dominate.

41

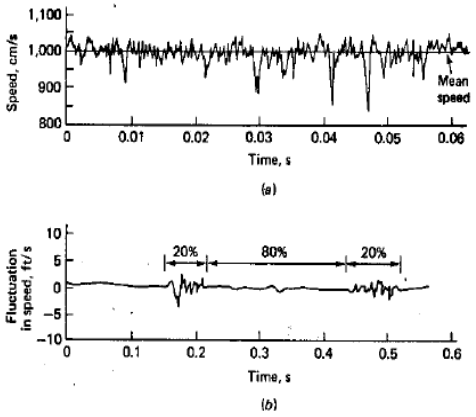

FIGURE 5-35
Hot-wire measurements showing turbulent velocity fluctuations: (*a*) typical trace of a single velocity component in a turbulent flow; (*b*) trace showing intermittent turbulence at the edge of a jet.

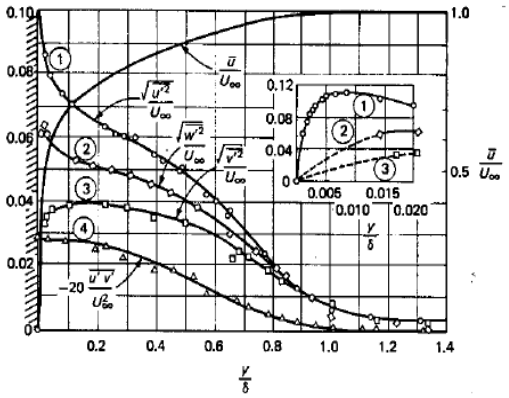

FIGURE 5-36
Flat-plate measurements of the fluctuating velocities u' (streamwise), v' (normal), and w' (lateral) and the turbulent shear $u'v'$. [*After Klebanoff (1955).*]

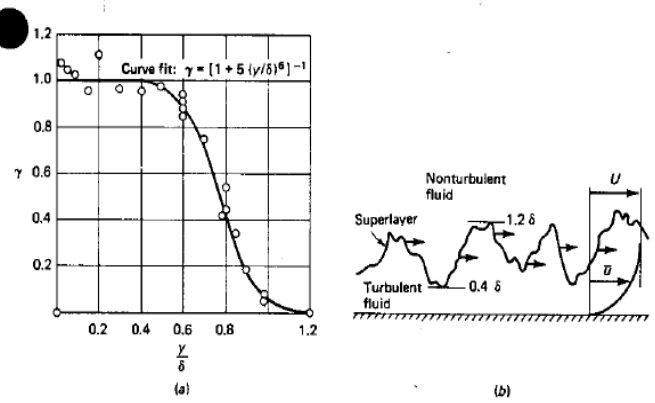

FIGURE 5-37
The phenomenon of intermittency in a turbulent boundary layer: (*a*) measured intermittency factors [*after Klebanoff (1955)*]; (*b*) the superlayer interface between turbulent and nonturbulent fluid.

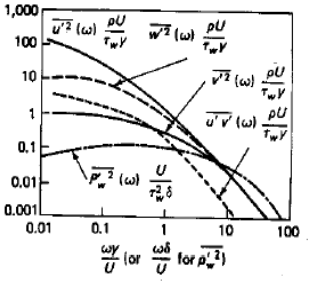

FIGURE 5-38
Measured frequency spectra of fluctuations in a low-speed turbulent boundary layer, scaled by inner-law variables (y, τ_w); u', v', w' from Bradshaw and Ferriss (1965); p'_w from Bakewell (1964).

Averages:

For turbulent flow $\underline{V}(\underline{x}, t)$, $p(\underline{x}, t)$ are random functions of time and must be evaluated statistically using averaging techniques: time, ensemble, phase, or conditional.

Time Averaging

For stationary flow, the mean is not a function of time and we can use time averaging.

$\bar{u} = \frac{1}{T}\int_{t_0}^{t_0+t} u(t)\,dt$ T > any significant period of $u' = u - \bar{u}$

(e.g. 1 sec. for wind tunnel and 20 min. for ocean)

Ensemble Averaging

For non-stationary flow, the mean is a function of time and ensemble averaging is used

$\bar{u}(t) = \frac{1}{N}\sum_{i=1}^{N} u^i(t)$ N is large enough that $\bar{u}$ independent

$u^i(t)$ = collection of experiments performed under identical conditions (also can be phase aligned for same t=o).

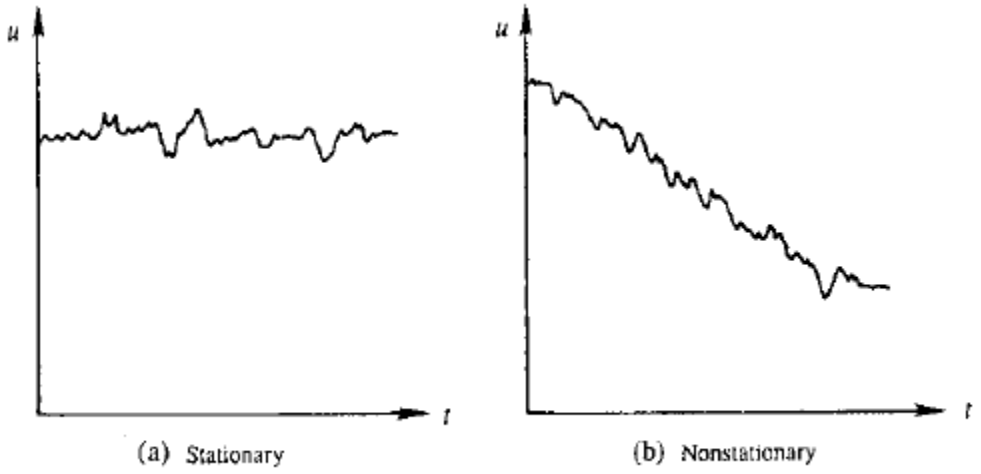

Fig. 12.2 Stationary and nonstationary time series.

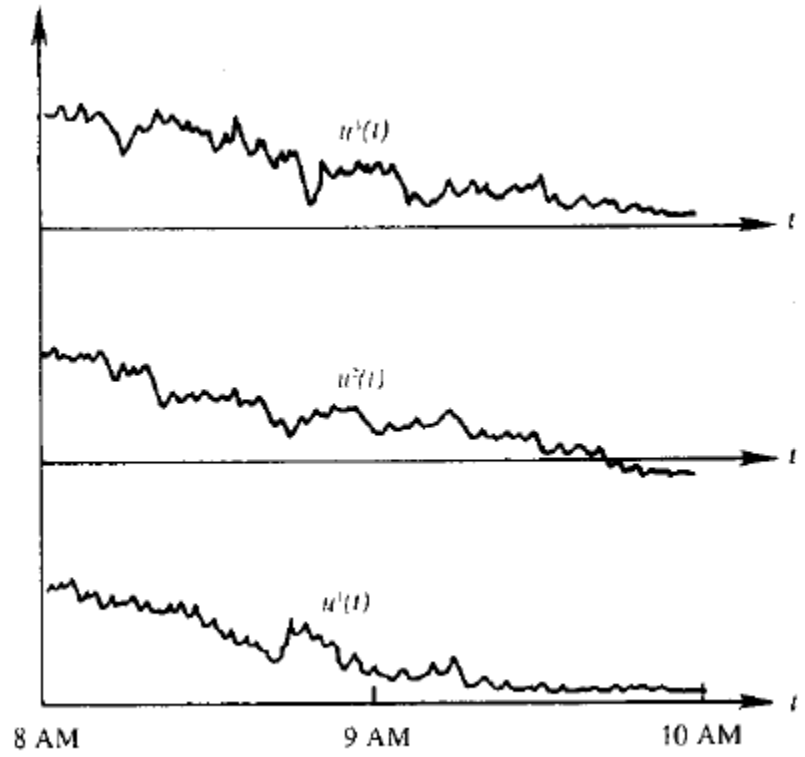

Fig. 12.3 An ensemble of functions $u(t)$.

Phase and Conditional Averaging

Similar to ensemble averaging, but for flows with dominant frequency content or other condition, which is used to align time series for some phase/condition. In this case triple velocity decomposition is used: $u = \bar{u} + u'' + u'$ where u'' is called organized oscillation. Phase/conditional averaging extracts all three components.

Averaging Rules:

$$f = \bar{f} + f' \qquad g = \bar{g} + g' \qquad s = x \text{ or } t$$

$$\bar{f}' = 0 \qquad \bar{\bar{f}} = \bar{f} \qquad \overline{f\bar{g}} = \bar{f}\bar{g} \qquad \overline{f'\bar{g}} = 0$$

$$\overline{f+g} = \bar{f} + \bar{g} \qquad \frac{\overline{\partial f}}{\partial s} = \frac{\partial \bar{f}}{\partial s} \qquad \overline{fg} = \bar{f}\bar{g} + \overline{f'g'}$$

$$\overline{\int f\, ds} = \int \bar{f}\, ds$$

Reynolds-Averaged Navier-Stokes Equations

For convenience of notation use uppercase for mean and lowercase for fluctuation in Reynolds decomposition.

$$\tilde{u}_i = U_i + u_i$$

$$\tilde{p} = P + p$$

$$\frac{\partial \tilde{u}_i}{\partial x_i} = 0$$

$$\frac{\partial \tilde{u}_i}{\partial t} + \tilde{u}_i \frac{\partial \tilde{u}_i}{\partial x_i} = -\frac{1}{\rho}\frac{\partial \tilde{p}}{\partial x_i} + \upsilon \frac{\partial^2 \tilde{u}_i}{\partial x_j \partial x_j} - g\delta_{i3}$$

→ NS equation

Mean Continuity Equation

$$\overline{\frac{\partial}{\partial x_i}(U_i + u_i)} = \frac{\partial U_i}{\partial x_i} + \frac{\partial \bar{u}_i}{\partial x_i} = \frac{\partial U_i}{\partial x_i} = 0$$

$$\frac{\partial \tilde{u}}{\partial x_i} = \frac{\partial U_i}{\partial x_i} + \frac{\partial u_i}{\partial x_i} = 0 \quad \rightarrow \quad \frac{\partial u_i}{\partial x_i} = 0$$

Both mean and fluctuation satisfy divergence = 0 condition.

Mean Momentum Equation

$$\frac{\partial}{\partial t}\left(U_i + u_i\right) + \left(U_j + u_j\right)\frac{\partial}{\partial x_j}\left(U_i + u_i\right) = -\frac{1}{\rho}\frac{\partial}{\partial x_i}\left(P + p\right) +$$

$$\frac{\partial^2}{\partial x_j x_j}\left(U_i + u_i\right) - g\delta_{i3}$$

$$\overline{\frac{\partial}{\partial t}\left(U_i + u_i\right)} = \frac{\partial U_i}{\partial t} + \frac{\partial \bar{u}_i}{\partial t} = \frac{\partial U_i}{\partial t}$$

$$\overline{\left(U_j + u_j\right)\frac{\partial}{\partial x_j}\left(U_i + u_i\right)} = U_j\frac{\partial U_i}{\partial x_j} + \cancel{U_j\frac{\partial \bar{u}_i}{\partial x_j}} + \cancel{\bar{u}_j\frac{\partial U_i}{\partial x_j}} + \overline{u_j\frac{\partial u_i}{\partial x_j}}$$

$$= U_j\frac{\partial U_i}{\partial x_j} + \frac{\partial}{\partial x_j}\overline{u_i u_j}$$

Since $$\frac{\partial}{\partial x_j}\overline{u_i u_j} = \cancel{\overline{u_i\frac{\partial u_j}{\partial x_j}}} + \overline{u_j\frac{\partial u_i}{\partial x_j}} = \overline{u_j\frac{\partial u_i}{\partial x_j}}$$

$$\overline{\frac{\partial}{\partial x_i}\left(P + p\right)} = \frac{\partial P}{\partial x_i} + \frac{\partial \bar{p}}{\partial x_i} = \frac{\partial P}{\partial x_i}$$

$$-\overline{g\delta_{i3}} = -g\delta_{i3}$$

$$\overline{\upsilon \frac{\partial^2}{\partial x_j{}^2}(U_i + u_i)} = \upsilon \frac{\partial^2 U_i}{\partial x_j^2} + \upsilon \frac{\partial^2 \bar{u}_i}{\partial x_j^2} = \upsilon \frac{\partial^2 U_i}{\partial x_j^2}$$

$$\frac{\partial U_i}{\partial t} + U_j \frac{\partial U_i}{\partial x_j} + \frac{\partial(\overline{u_i u_j})}{\partial x_j} = -\frac{1}{\rho}\frac{\partial P}{\partial x_i} + \upsilon \frac{\partial^2}{\partial x_j^2} U_i - g\delta_{i3}$$

Or $$\frac{DU_i}{Dt} = -\frac{1}{\rho}\frac{\partial P}{\partial x_i} - g\delta_{i3} + \frac{\partial}{\partial x_j}\left[\upsilon \frac{\partial U_i}{\partial x_j} - \overline{u_i u_j}\right]$$

Or $$\frac{DU_i}{Dt} = -g\delta_{i3} + \frac{1}{\rho}\frac{\partial}{\partial x_i}\bar{\sigma}_{ij}$$

$$\bar{\sigma} = -P\delta_{ij} + \mu\left(\frac{\partial U_i}{\partial x_j} + \frac{\partial U_j}{\partial x_i}\right) - \rho\overline{u_i u_j}$$

with $$\frac{\partial U_i}{\partial x_i} = 0$$

→ RANS Equations

The difference between the NS and RANS equations is the Reynolds stresses $-\rho\overline{u_i u_j}$, which acts like additional stress.

$-\rho\overline{u_i u_j} = -\rho\overline{u_j u_i}$ (i.e. Reynolds stresses are symmetric)

$$= \begin{bmatrix} -\rho\overline{u^2} & -\rho\overline{uv} & -\rho\overline{uw} \\ -\rho\overline{uv} & -\rho\overline{v^2} & -\rho\overline{vw} \\ -\rho\overline{uw} & -\rho\overline{vw} & -\rho\overline{w^2} \end{bmatrix}$$

$\overline{u_i^2}$ are normal stresses

$\overline{u_i u_j}$ $i \neq j$ are shear stresses

6 new unknowns

For homogeneous/isotropic turbulence $\overline{u_i u_j}$ $i \neq j = 0$ and $\overline{u^2} = \overline{v^2} = \overline{w^2} =$ constant; however, turbulence is generally non-isotropic.

For example, consider shear flow with $\frac{dU}{dy} > 0$ as below,

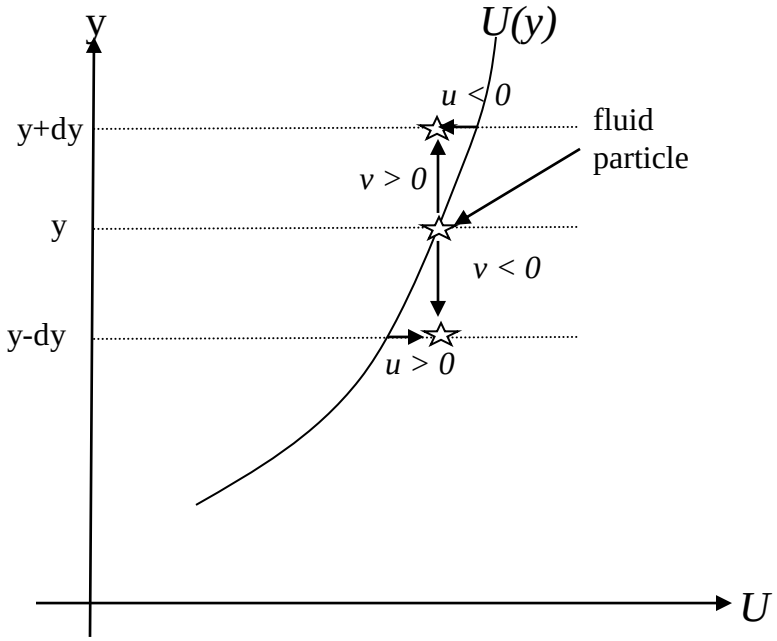

The fluid velocity is: $\underline{V} = (U+u, v, w)$

Assuming that fluid particle retains its velocity $\underline{V}$ from y to $y \pm dy$ gives,

$$\left.\begin{array}{l} v>0 \rightarrow u<0 \\ v<0 \rightarrow u>0 \end{array}\right\} \rightarrow \overline{uv}<0$$

x-momentum tends towards decreasing y as turbulence diffuses gradients and decreases $\frac{dU}{dy}$

x-momentum transport in y direction, i.e., across y = constant AA per unit area

$M_{xy} = \int \rho \tilde{u} \underline{V} \cdot \underline{n}\, dA$, where $\tilde{u} = (U + u)$

$$\frac{d\overline{M_{xy}}}{dA} = \rho\overline{(U+u)v} = \rho U\bar{v} + \rho\overline{uv} = \rho\overline{uv}$$

i.e $\rho\overline{u_i u_j}$ = average flux of j-momentum in i-direction = average flux of i-momentum in j-direction

Closure Problem:

1. RANS equations differ from the NS equations due to the Reynolds stress terms
2. RANS equations are for the mean flow (U_i, P); thus, represent 4 equations with 10 unknowns due to the additional 6 unknown Reynolds stresses $\overline{u}_i\overline{u}_j$
3. Equations can be derived for $\overline{u}_i\overline{u}_j$ by summing products of velocity and momentum components and time averaging, but these include additionally 10 triple product $\overline{u}_i\overline{u}_j\overline{u}_l$ unknowns. Triple products represent Reynolds stress transport.
4. Again equations for triple products can be derived that involve higher order correlations leading to fact that RANS equations are inherently non-deterministic, which requires turbulence modeling.
5. Turbulence closure models render deterministic RANS solutions.
6. The NS and RANS equations have paradox that NS equations are deterministic but have nondeterministic solutions for turbulent flow due to inherent stochastic nature of turbulence, whereas the RANS equations are nondeterministic, but have deterministic solutions due to turbulence closure models.

Turbulent Kinetic Energy Equation

$k = \frac{1}{2}\overline{u_i^2} = \frac{1}{2}\left(\overline{u^2} + \overline{v^2} + \overline{w^2}\right)$ = turbulent kinetic energy

Subtracting NS equation for $\tilde{u}_i$ and RANS equation for U_i results in equation for u_i:

$$\frac{\partial u_i}{\partial t} + U_j \frac{\partial u_i}{\partial x_j} + u_j \frac{\partial U_i}{\partial x_j} + u_j \frac{\partial u_i}{\partial x_j} - \frac{\partial}{\partial x_j}(\overline{u_i u_j}) = -\frac{1}{\rho}\frac{\partial p}{\partial x_i} + \upsilon \frac{\partial^2 u_i}{\partial x_j^2}$$

Multiply by u_i and average

$$\frac{Dk}{Dt} = \underbrace{-\frac{1}{\rho}\frac{\partial}{\partial x_j}\overline{pu_j}}_{I} \underbrace{-\frac{1}{2}\frac{\partial}{\partial x_j}\overline{u_i^2 u_j}}_{II} + \underbrace{2\upsilon\frac{\partial}{\partial x_j}\overline{u_i e_{ij}}}_{III} \underbrace{-\overline{u_i u_j}\frac{\partial U_i}{\partial x_j}}_{IV} \underbrace{-2\upsilon\overline{e_{ij}e_{ji}}}_{V}$$

Where $\underbrace{\frac{Dk}{Dt} = \frac{\partial k}{\partial t} + U_j \frac{\partial k}{\partial x_j}}_{VI}$ and $e_{ij} = \frac{1}{2}\frac{\partial u_i}{\partial x_j}\frac{\partial u_j}{\partial x_i}$

I =pressure transport
II= turbulent transport
III=viscous diffusion
IV = shear production (usually > 0) represents loss of mean kinetic energy and gain of turbulent kinetic energy due to interactions of $\overline{u_i u_j}$ and $\frac{\partial U_i}{\partial x_j}$.
V = viscous dissipation = ε
VI= turbulent convection

Recall previous discussions of energy cascade and dissipation:

Energy fed from mean flow to largest eddies and cascades to smallest eddies where dissipation takes place

Kinetic energy = k = u_o^2
$\tau_0 = \frac{l_0}{u_0}$ = turn over time
$\varepsilon = \frac{u_0^2}{\tau_0} = \frac{u_0^3}{l_0}$ $l_0 = L_\delta$ = width of flow (i.e. size of largest eddy)

Kolmogorov Hypothesis:

(1) local isotropy: for large Re, micro-scale $\ell << \ell_0$ turbulence structures are isotropic.

(2) first similarity: for large Re, micro-scale has universal form uniquely determined by υ and ε.

$\eta = \left(\upsilon^3/\varepsilon\right)^{1/4}$ length $\eta/l_0 = \mathrm{Re}^{-3/4}$

$u_\eta = (\varepsilon\upsilon)^{1/4}$ velocity $u_\eta/u_0 = \mathrm{Re}^{-1/4}$

$\tau_\eta = (\upsilon/\varepsilon)^{1/2}$ time $\underbrace{\tau_\eta/\tau_0 = \mathrm{Re}^{-1/2}}$

Micro-scale<<large scale

Also shows that as Re increases, the range of scales increase.

(3) second similarity: for large Re, intermediate scale has a universal form uniquely determined by ε and independent of υ.

(2) and (3) are called universal equilibrium range in distinction from non-isotropic energy-containing range. (2) is the dissipation range and (3) is the inertial subrange.

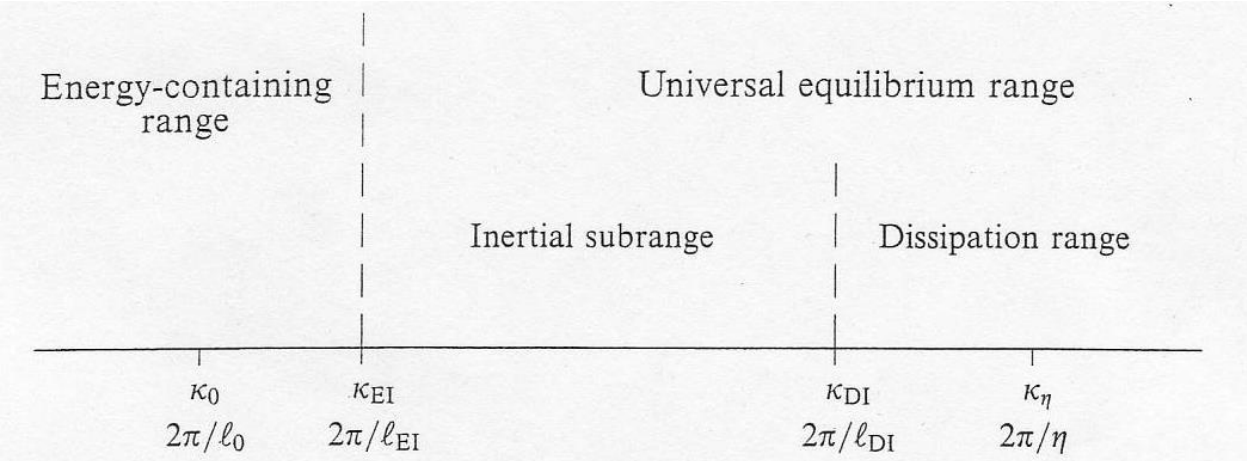

Fig. 6.12. Wavenumbers (on a logarithmic scale) at very high Reynolds number showing the various ranges.

Spectrum of turbulence in the inertial subrange

$\overline{u^2} = \int_0^\infty S(k)\,dk$ k = wave number in inertial subrange.

$S = A\varepsilon^{2/3}k^{-5/3}$

For $l_0^{-1} << k << \eta^{-1}$ (based on dimensional analysis)

A ~ 1.5 Called Kolmogorov $k^{-5/3}$ law

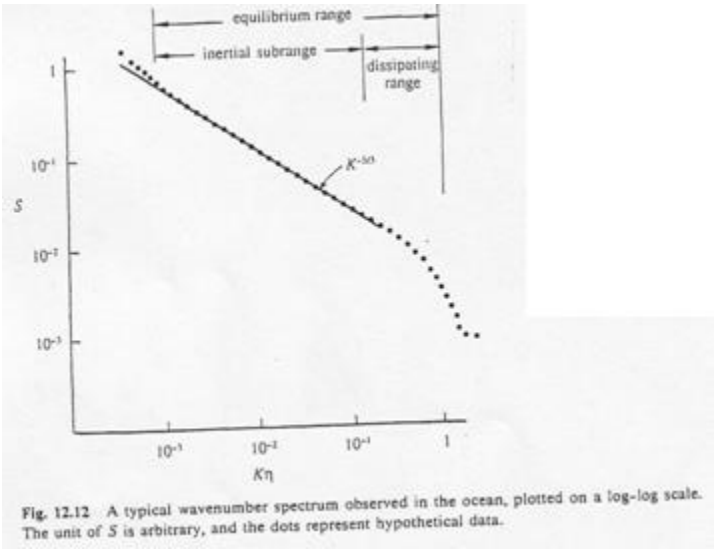

Fig. 12.12 A typical wavenumber spectrum observed in the ocean, plotted on a log-log scale. The unit of S is arbitrary, and the dots represent hypothetical data.

Velocity Profiles: Inner, Outer, and Overlap Layers

Detailed examination of turbulent boundary layer velocity profiles indicates the existence of a three-layer structure:

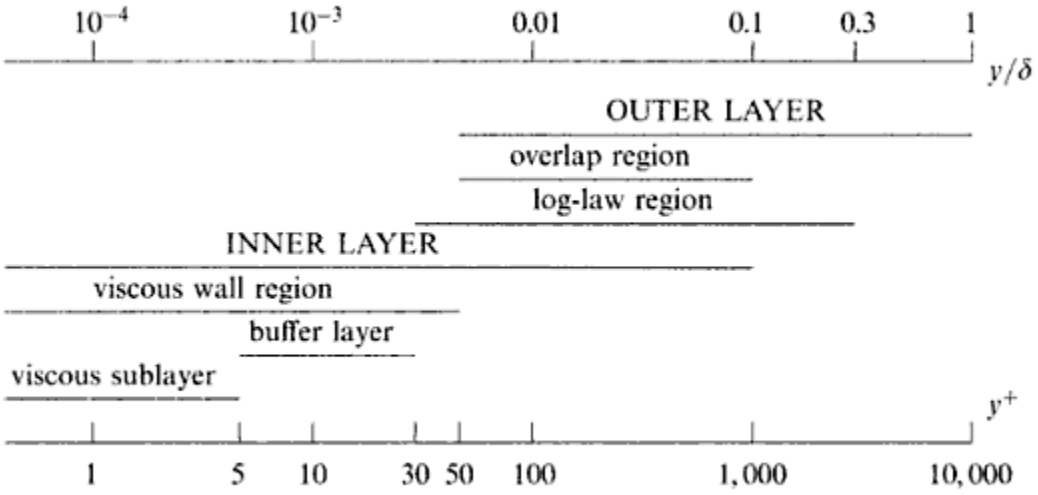

Fig. 7.8. A sketch showing the various wall regions and layers defined in terms of $y^+ = y/\delta_v$ and y/δ, for turbulent channel flow at high Reynolds number ($Re_\tau = 10^4$).

Figure: Pope (2000, Fig. 7.8)

(1) A thin inner layer close to the wall, which is governed by molecular viscous scales, and independent of boundary layer thickness δ, free-stream velocity U_e and pressure gradient.

(2) An outer layer where the flow is governed by turbulent shear stresses,δ, U_e and pressure gradient, but independent of ν.

(3) An overlap layer which smoothly connects inner and outer regions. In this region both molecular and turbulent stresses and pressure gradient are important.

Considerable more information is obtained from the dimensional analysis and confirmed by experiment.

Inner layer: $U = f(\tau_w, \rho, \mu, y)$

$$U^+ = \frac{U}{u^*} = f(\frac{yu^*}{\nu}) \qquad u^* = \sqrt{\tau_w / \rho} \quad \text{Wall shear velocity}$$

$$= f(y^+)$$

U^+, y^+ are called inner-wall variables

Note that the inner layer is independent of δ or r_0, for boundary layer and pipe flow, respectively.

Outer Layer: $\underbrace{U_e - U}_{velocity\ defect} = g(\tau_w, \rho, y, \delta)$ for $p_x = 0$

$$\frac{U_e - U}{u^*} = g(\eta) \qquad \text{where } \eta = y/\delta$$

Note that the outer layer is independent of μ.

Overlap layer: both laws are valid

In this region both log-law and outer layer is valid.

It is not that difficult to show that for both laws to overlap, f and g are logarithmic functions.

Inner region:

$$\frac{dU}{dy} = \frac{u^{*2}}{\nu}\frac{df}{dy^+}$$

Outer region:

$$\frac{dU}{dy} = \frac{u^*}{\delta}\frac{dg}{d\eta}$$

$$\underbrace{\frac{y}{u^*}\frac{u^{*2}}{\nu}\frac{df}{dy^+}}_{f(y+)} = \underbrace{\frac{y}{u^*}\frac{u^*}{\delta}\frac{dg}{d\eta}}_{g(\eta)}$$; valid at large y^+ and small η.

Therefore, both sides must equal universal constant, κ^{-1}

$$f(y^+) = \frac{1}{\kappa}\ln y^+ + B = U/u^* \quad \text{(inner variables)}$$

$$g(\eta) = \frac{1}{\kappa}\ln\eta + A = \frac{U_e - U}{u^*} \quad \text{(outer variables)}$$

κ, A, and B are pure dimensionless constants

Values vary somewhat depending on different exp. arrangements

κ	=	0.41	Von Karman constant	
B	=	5.5		
A	=	2.35	BL flow	*The difference is due to loss of intermittency in duct flow. A = 0 means small outer layer*
	=	0.65	pipe flow	

The validity of these laws has been established experimentally as shown in Fig. 6-9, which shows the profiles of Fig 6-8 in inner-law variable format. All the profiles, with the exception of the one for separated flow, are seen to follow the expected behavior. In the case of separated flow, scaling the profile with u* is inappropriate since u* ~ 0.

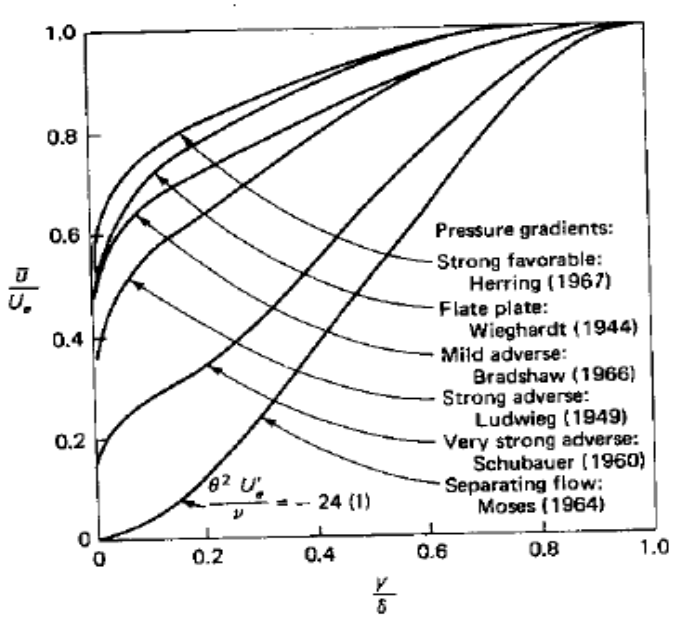

FIGURE 6-8
Experimental turbulent-boundary-layer velocity profiles for various pressure gradients. [*Data from Coles and Hirst (1968).*]

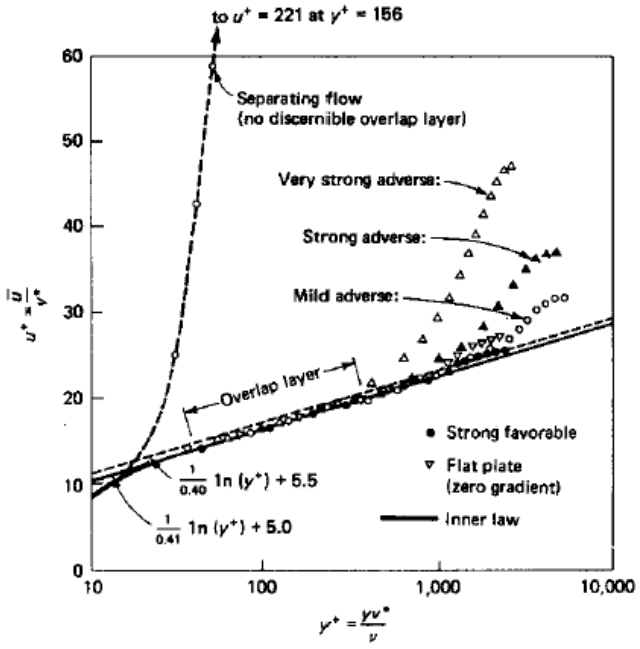

FIGURE 6-9
Replot of the velocity profiles of Fig. 6-8 using inner-law variables y^+ and u^+.

Details of Inner Layer

Neglecting inertia and pressure forces in the 2D turbulent boundary layer equation we get:

$$\frac{d}{dy}(\mu\left(\frac{dU}{dy}\right) - \rho\overline{uv}\,) = 0$$

$$\rightarrow \qquad \mu\left(\frac{dU}{dy}\right) - \rho\overline{uv} = \tau_t$$

The total shear stress is the sum of viscous and turbulent stresses. Very near the wall y→0, the turbulent stress vanishes. Sublayer region:

$$\lim_{y\to 0} \mu\left(\frac{dU}{dy}\right) - \rho\overline{uv} = \mu\left(\frac{dU}{dy}\right)_{y=0} = \tau_w$$

From the inner layer velocity profile:

$$\left(\frac{dU}{dy}\right)_{y=0} = \frac{u^{*2}}{\nu}\frac{df(y^+)}{dy^+} = \frac{\tau_w}{\mu}$$

$$\frac{df(y^+)}{dy^+} = 1 \quad \rightarrow f(y^+) = y^+ + C$$

No slip condition at $y = 0$ requires $C = 0$.

Sublayer: $U^+ = y^+$ valid for $y^+ \leq 5$

Buffer layer: Merges smoothly the viscosity-dominated sub-layer and turbulence-dominated log-layer in the region $5< y^+ \leq 30$.

Unified Inner layer: There are several ways to obtain composite of sub-/buffer and log-layers.

Evaluating the RANS equation near the wall using μ_t turbulence model shows that:

$$\mu_t \sim y^3 \qquad y \rightarrow 0$$

Several expressions which satisfy this requirement have been derived and are commonly used in turbulent-flow analysis. That is:

$$\mu_t = \mu\kappa e^{-\kappa B}\left[e^{\kappa U^+} - 1 - \kappa U^+ - \frac{\left(\kappa U^+\right)^2}{2}\right]$$

Assuming the total shear is constant very near to the wall a composite formula which is valid in the sub-layer, blending layer, and logarithmic-overlap regions is obtained

$$U^+ = y^+ - e^{-\kappa B}\left[e^{\kappa u^+} - 1 - \kappa U^+ - \frac{\left(\kappa U^+\right)^2}{2} - \frac{\left(\kappa U^+\right)^3}{6}\right]$$

Fig. 6-11 shows a comparison of this equation with experimental data obtained very close to the wall. The agreement is excellent. It should be recognized that obtaining data this close to the wall is very difficult.

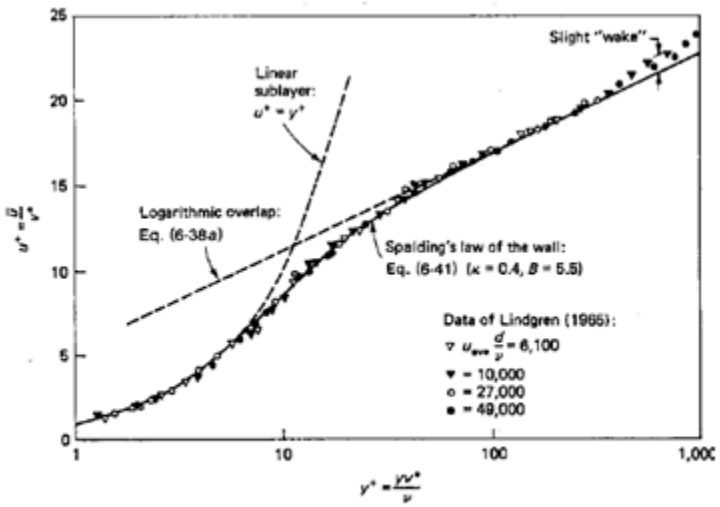

FIGURE 6-11
Comparison of Spalding's inner-law expression with the pipe-flow data of Lindgren (1965).

Details of the Outer Law

At the end of the overlap region the velocity defect is given approximately by:

$$\frac{U_e - U}{u^*} = 9.6(1-\eta)^2$$

With pressure gradient included, the outer law becomes (Fig. 6-10):

$$\frac{U_e - U}{u^*} = g(\eta, \beta)$$

$$\eta = y/\delta \qquad \beta = \frac{\delta^*}{\tau_w}\frac{dp_c}{dx} = \text{Clauser's equilibrium parameter}$$

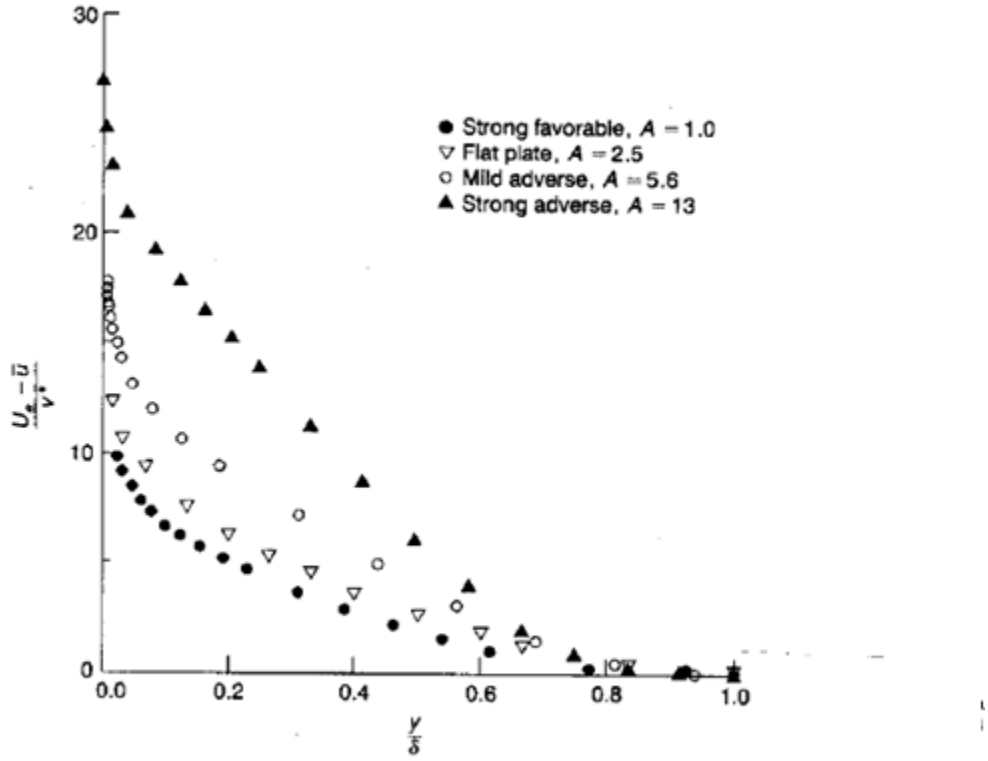

FIGURE 6-10
Replot of the velocity profiles of Fig. 6-8 using outer-law variables from Eq. (6-36). Success is not evident because each profile has a different value of the parameter ξ.

Clauser (1954,1956):

BL's with different p_x but constant β are in equilibrium, i.e., can be scaled with a single parameter:

$$\frac{U_e - U}{u^*} \quad \text{vs.} \quad y/\Delta$$

$$\Delta = defect\ thickness = \int_0^\infty \frac{U_e - U}{u^*} dy = \delta^* \lambda$$

$$\lambda = \sqrt{2/C_f}$$

Also, G = Clauser Shape parameter

$$= \frac{1}{\Delta}\int_0^\infty \left(\frac{U_e - U}{u^*}\right)^2 dy \qquad = \qquad \underbrace{6.1\sqrt{\beta + 1.81} - 1.7}_{Curve-fit\ \ by\ Mach}$$

Which is related to the usual shape parameter by

$$H = (1 - G/\lambda)^{-1} \neq const.\ due\ to\ \lambda = \lambda(x)$$

Finally, Clauser showed that the outer layer has a wake-like structure such that

$$\mu_t \approx 0.016 \rho U_e \delta^*$$

Mellor and Gibson (1966) combined these equations into a theory for equilibrium outer law profiles with excellent agreement with experimental data: Fig. 6-12

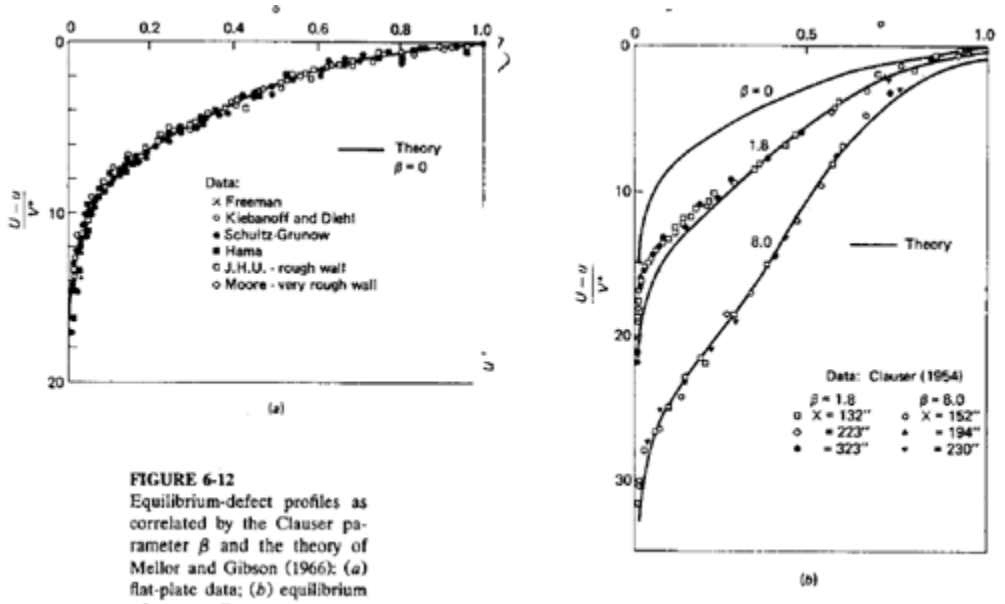

FIGURE 6-12
Equilibrium-defect profiles as correlated by the Clauser parameter β and the theory of Mellor and Gibson (1966): (*a*) flat-plate data; (*b*) equilibrium adverse gradients.

Coles (1956):

A weakness of the Clauser approach is that the equilibrium profiles do not have any recognizable shape. This was resolved by Coles who showed that:

Deviations above log-overlap layer

$$\frac{U^+ - 2.5\ln y^+ - 5.5}{U_e^+ - 2.5\ln \delta^+ - 5.5} \approx \frac{1}{2}W(y/\delta)$$

Max deviation at δ

Single wake-like function of y/δ

$$W = wake\ \ function = \underbrace{2\sin^2\left(\frac{\pi}{2}\frac{y}{\delta}\right)}_{curve\ fit} = 3\eta^2 - 2\eta^3,\ \eta = y/\delta$$

Thus, it is possible to derive a composite which covers both the overlap and outer layers, as shown in Fig. 6-13.

$$U^+ = \frac{1}{\kappa}\ln y^+ + B + \frac{\pi}{\kappa}W(y/\delta)$$

$$\pi = wake\ \ parameter\ = \pi(\beta)$$

$$= 0.8(\beta + 0.5)^{0.75} \longrightarrow \quad (curve\ fit\ for\ data)$$

Note the agreement of Coles' wake law even for $\beta \neq$ constant. Bl's is quite good.

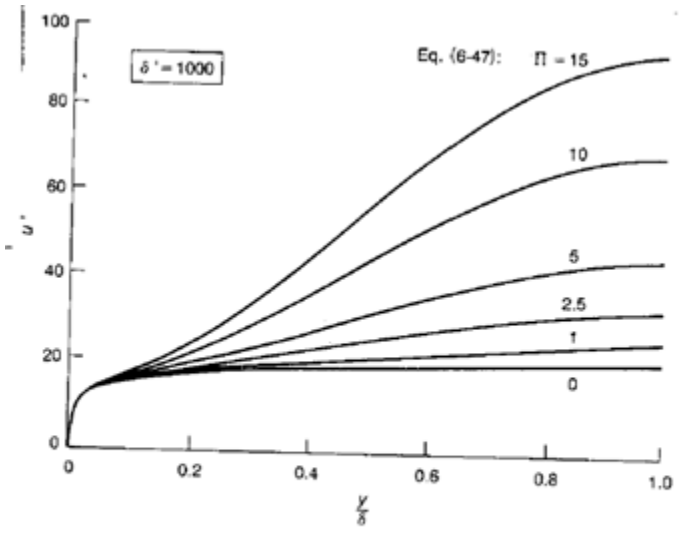

FIGURE 6-13
Turbulent velocity profiles computed from the Coles wall-wake formula, Eq. (6-47), assumin $\delta^+ = 1000$. The curve for $\Pi = 0$ is the pure law of the wall from Eq. (6-41).

We see that the behavior in the outer layer is more complex than that of the inner layer due to pressure gradient effects. In general, the above velocity profile correlations are extremely valuable both in providing physical insight and in providing approximate solutions

for simple wall bounded geometries: pipe, channel flow and flat plate boundary layer. Furthermore, such correlations have been extended through the use of additional parameters to provide velocity formulas for use with integral methods for solving the BL equations for arbitrary p_x.

Summary of Inner, Outer, and Overlap Layers

Mean velocity correlations

Inner layer:

$$U^+ = f(y^+)$$

$$U^+ = U/u^* \quad y^+ = y/u^* \quad u^* = \sqrt{\tau_w/\rho}$$

Sub-layer: $U^+ = y^+$ for $0 \le y^+ \le 5$

Buffer layer: where sub-layer merges smoothly with log-law region for $5 < y^+ \le 30$

Outer Layer:

$$\frac{U_e - U}{u^*} = g(\eta, \beta) \qquad \eta = y/\delta, \qquad \beta = \frac{\delta^*}{\tau_w} p_x$$

for $\eta > 0.1$

Overlap layer (log region):

$$U^+ = \frac{1}{\kappa}\ln y^+ + B \qquad \text{inner variables}$$

$$\frac{U_e - U}{u^*} = -\frac{1}{\kappa}\ln\eta + A \qquad \text{outer variables}$$

for $y^+ > 30$ and $\eta \le 0.3$

Composite Inner/Overlap layer correlation

$$U^+ = y^+ - e^{-\kappa b}\left[e^{\kappa b} - 1 - \kappa U^+ - \frac{(\kappa U^+)^2}{2} - \frac{(\kappa U^+)^3}{6}\right]$$

for $0 < y^+ \le 50$

Composite Overlap/Outer layer correlation

$$U^+ = \frac{1}{\kappa}\ln y^+ + B + \frac{2\pi}{\kappa}W(\eta) \qquad W = \sin^2\left(\frac{\pi}{2}\eta\right) = 3\eta^2 - 2\eta^3$$

$$\pi = 0.8(\beta + 0.5)^{0.75}$$

for $y^+ > 50$

Reynolds Number Dependence of Mean-Velocity Profiles and Reynolds stresses

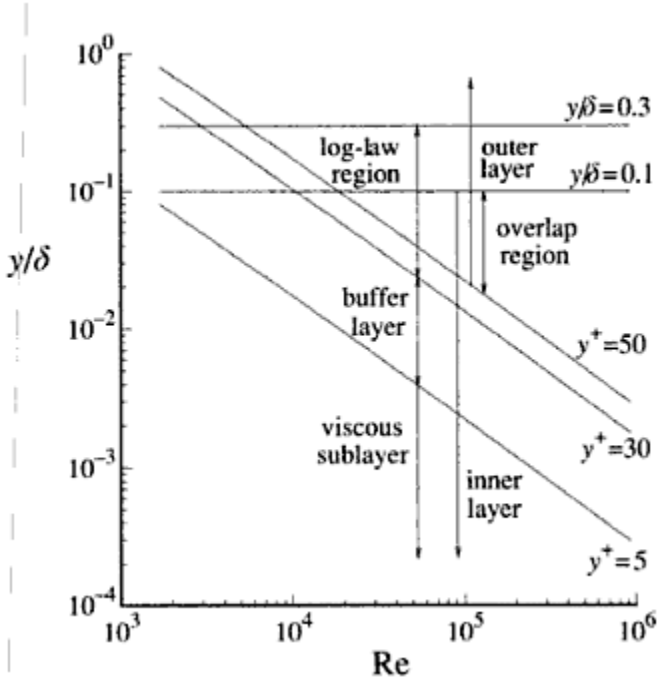

Figure: Pope (2000, Fig. 7.13)

1. Inner/overlap U^+ scaling shows similarity; extent of overlap region (i.e. similarity) increases with Re.

2. Outer layer for $p_x = 0$ may asymptotically approach similarity for large Re as shown by $\Delta U^+ (= 2\pi/k)$ vs. Re_θ, but controversial due to lack of data for Re_θ 5 x 10^4.

3. The normalized Reynolds stresses $\overline{u_i u_j}/k$, production-dissipation ratio and the normalized mean shear stress are somewhat uniform in the log-law region. Experiments in flat plate boundary layer,

pipe and channel flow shows k = 3.34 - 3.43 u^{*2} in lower part of log-law region.

4. Decay of $k \sim y^2$ near the wall.

5. Streamwise turbulence intensity $u^+ = \overline{u^2}/u^*$ vs. y^+ shows similarity for $0 \le y^+ \le 15$ (i.e., just beyond the point of k_{max}, $y^+ = 12$), but u^+ increases with Re_θ.

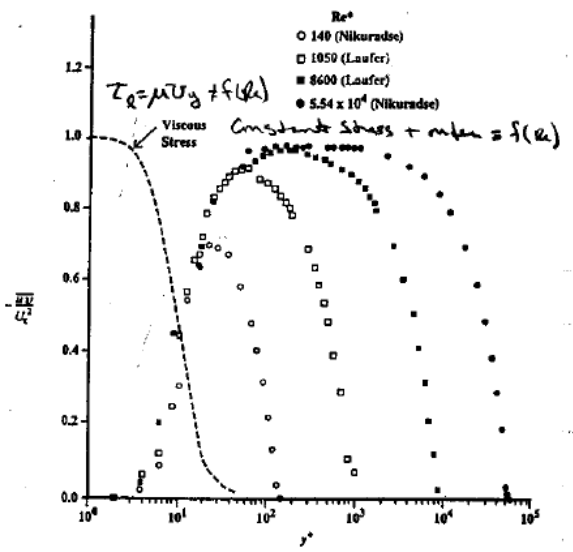

Fig 5. Distribution of viscous and turbulence shear stresses in wall-bounded flows (from Sreenivasan, 1989).

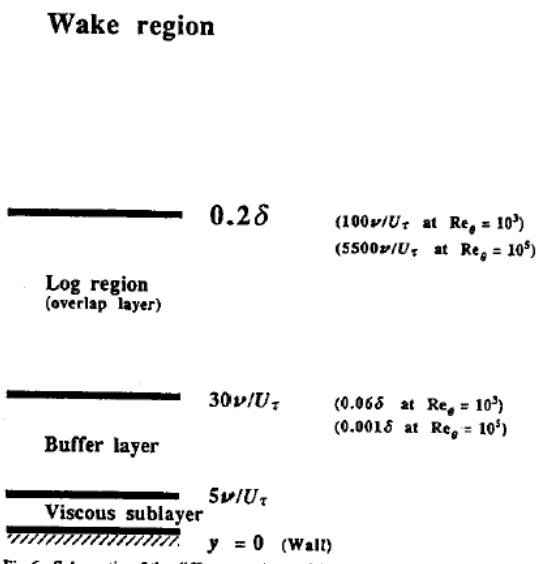

Fig 6. Schematic of the different regions within a wall-bounded flow at typical low and high Reynolds numbers.

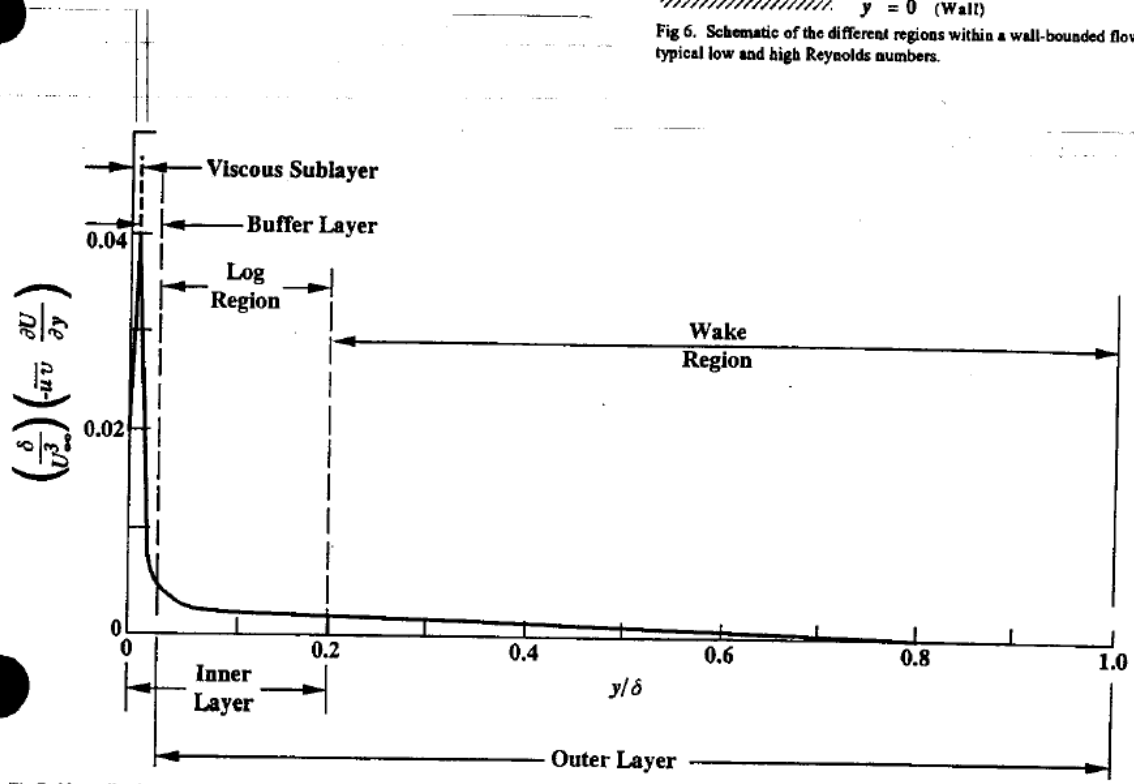

Fig 7. Normalized turbulence kinetic energy production rate as a function of normal distance from the wall. Data for a typical laboratory flat-plate boundary layer (from Kline *et al*, 1967).

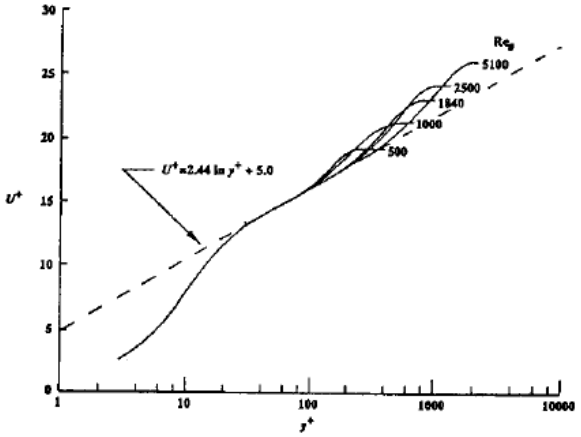

Fig 10. Comparison of mean-velocity profiles with logarithmic law at low Reynolds numbers. Boundary layer data from Purtell *et al* (1981).

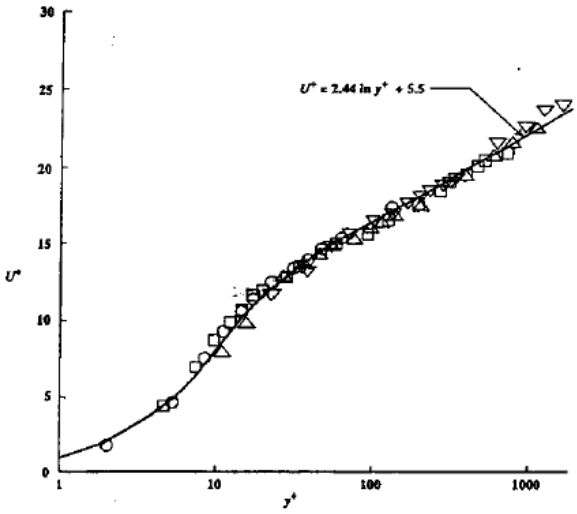

Fig 12. Mean-velocity profiles non-dimensionalized on inner variables. Channel flow data from Wei and Willmarth (1989).

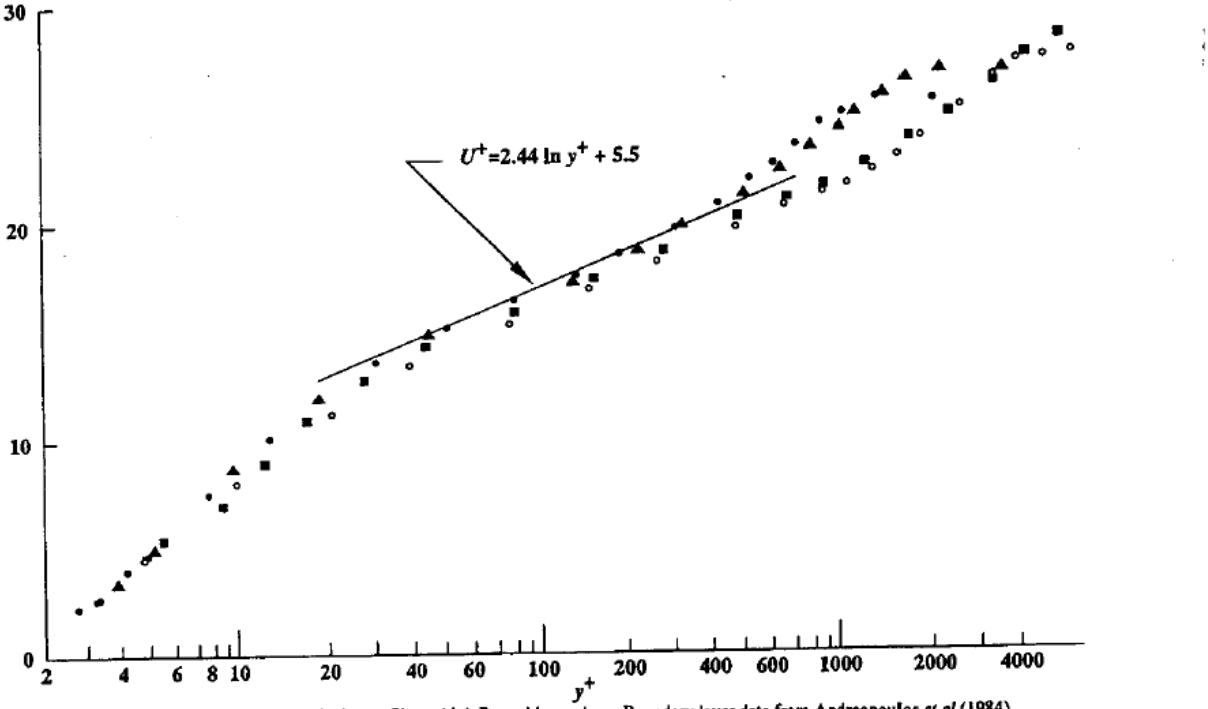

Fig 11. Non-dimensionalized mean-velocity profiles at high Reynolds numbers. Boundary layer data from Andreopoulos *et al* (1984).

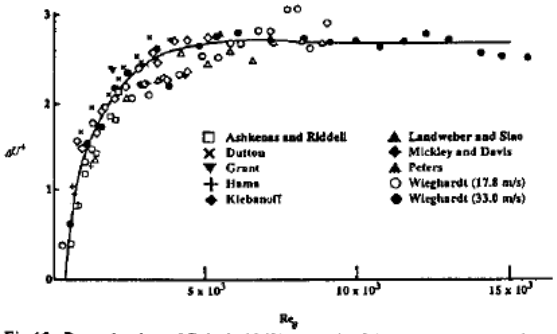

Fig 13. Reproduction of Coles' (1962) strength of the wake component in equilibrium turbulent boundary layers at low Reynolds numbers.

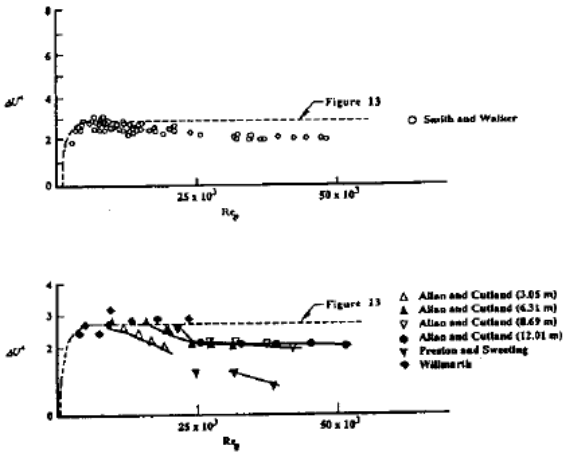

Fig 14. Reproduction of Coles' (1962) strength of the wake component at large Reynolds numbers.

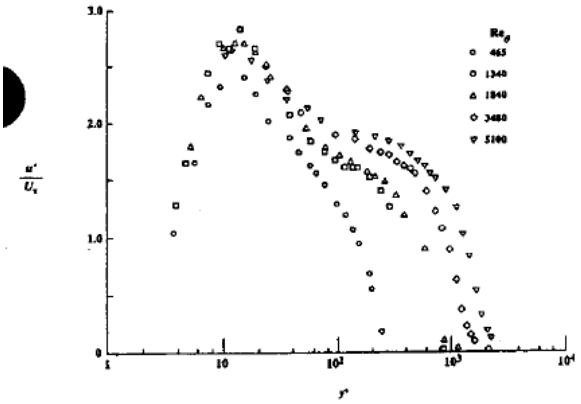

Fig 18. Variation of the distribution of turbulence intensity in wall variables with Reynolds number. Boundary layer data from Purtell *et al* (1981).

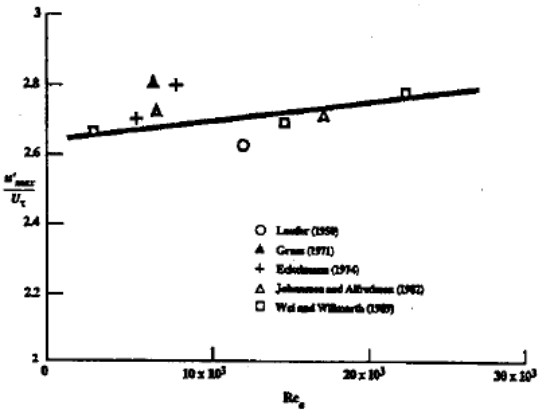

Fig 27. Peak value of *u*-turbulence intensity in two-dimensional channel flows. The plot, from five different experiments, demonstrates the effect of outer layer scales on inner-layer turbulence. Solid line represents the mean trend (from Bandyopadhyay, 1991).

67

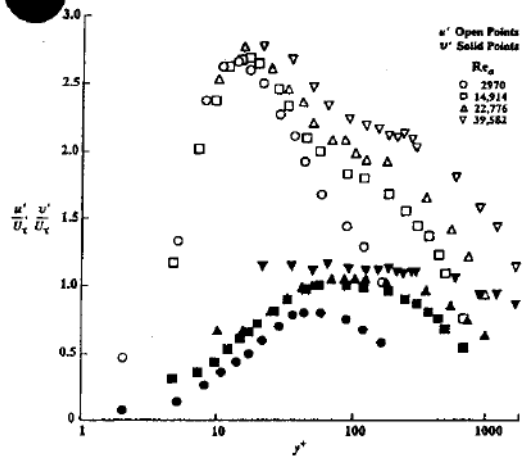

Fig 25. Profiles of turbulence intensity in streamwise direction (open points) and direction normal to wall (solid points), non-dimensionalized on inner variables. Channel flow data of Wei and Willmarth (1989).

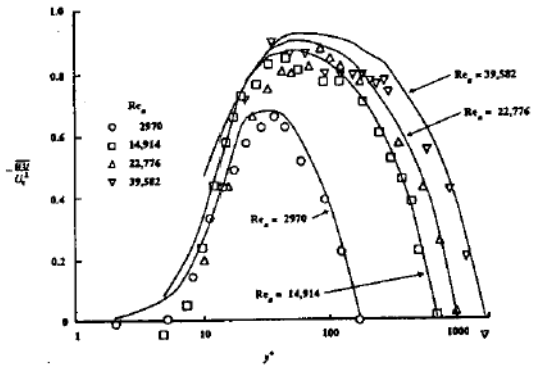

Fig 31. Reynolds stress profiles non-dimensionalized on inner variables. Channel flow data of Wei and Willmarth (1989) at four different Reynolds numbers. Solid line represents momentum balance calculations.

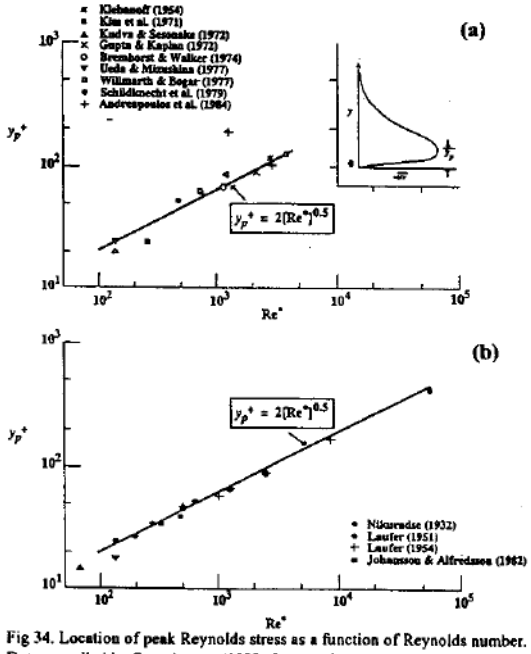

Fig 34. Location of peak Reynolds stress as a function of Reynolds number. Data compiled by Sreenivasan (1988) from various wall-bounded flow experiments. Solid lines are least-square fit: (a) Directly measured Reynolds stress; (b) Computed from measured mean velocity. The lowermost two data points correspond to the critical layer position in typical transitional flows.